

Field-effect Modulation of Anomalous Hall Effect in Diluted Ferromagnetic Topological Insulator Epitaxial Films

Cui-Zu Chang,^{1, 2, 3*} Min-Hao Liu,² Zuo-Cheng Zhang,² Yayu Wang,² Ke He,¹ and Qi-Kun Xue^{2, 1}

¹ State Key Laboratory of Low-Dimensional Quantum Physics, Department of Physics,

Tsinghua University, Beijing 100084, China

² Beijing National Laboratory for Condensed Matter Physics, Institute of Physics,

Chinese Academy of Sciences, Beijing 100190, China

³ Francis Bitter Magnet Lab, Massachusetts Institute of Technology, Cambridge, MA 02139, USA

Email: czchang@mit.edu (C. Z. C)

High quality chromium (Cr) doped three-dimensional topological insulator (TI) Sb_2Te_3 films are grown via molecular beam epitaxy on heat-treated insulating $\text{SrTiO}_3(111)$ substrates. We report that the Dirac surface states are insensitive to Cr doping, and a perfect robust long-range ferromagnetic order is unveiled in epitaxial $\text{Sb}_{2-x}\text{Cr}_x\text{Te}_3$ films. The anomalous Hall effect is modulated by applying a bottom gate, contrary to the ferromagnetism in conventional diluted magnetic semiconductors (DMSs), here the coercivity field is not significantly changed with decreasing carrier density. Carrier-independent ferromagnetism heralds $\text{Sb}_{2-x}\text{Cr}_x\text{Te}_3$ films as the base candidate TI material to realize the quantum anomalous Hall (QAH) effect. These results also indicate the potential of controlling anomalous Hall voltage in future TI-based magneto-electronics and spintronics.

Topological insulators (TIs) are a recently discovered class of quantum coherent materials with an insulating bulk but metallic surfaces/edges. TI's metallic Dirac surface states (DSSs) show many fascinating properties including: an extraordinary spin texture, massless Dirac fermions, and robust stability.¹⁻³ The tetradymite semiconductor diantimony tritelluride (Sb_2Te_3) has been theoretically predicted, and experimentally observed, to be a three-dimensional (3D) TI with single Dirac cone⁴⁻⁶ that lies well inside the bulk gap. Sb_2Te_3 is always *p*-type due to the formation of native antisite defects.⁵⁻⁷ Sb_2Te_3 also belongs to the family of narrow-bandgap semiconductors, with a bulk gap of ~ 260 meV. Doping transition metal elements in conventional narrow-bandgap semiconductors usually induces ferromagnetism. These doping-induced ferromagnetic systems are known as diluted magnetic semiconductors (DMSs).²² We doped the matrix of Sb_2Te_3 with varying amounts of chromium (Cr), which can lead to a robust long-range ferromagnetic state.⁸ It is well known that, time-reversal symmetry breaking in 3D TI-based tetradymite-type DMSs yields novel electronic and magnetic properties including: gap opening at the Dirac point (DP);⁹ the quantum anomalous Hall (QAH) effect;¹⁰⁻¹² the topological magneto-electric (TME) effect;¹¹ and image magnetic monopoles.¹³

The ultrathin Cr-doped Sb_2Te_3 films were grown by molecular beam epitaxy (MBE) in an ultra-high vacuum (UHV) with a base pressure better than 2×10^{-10} mbar.¹⁴ Insulating commercial $\text{SrTiO}_3(111)$ substrates were used because their large dielectric constant after heat treating ($\kappa \sim 30000$ at temperature $T \sim 2\text{K}$), enables tuning carrier density (n_{2D}) with a bottom gate bias (V_g), even with a thick ($\sim 0.5\text{mm}$) substrate.¹⁵ High purity Sb (99.9999%), Te (99.9999%) and Cr (99.999%) were simultaneously evaporated from standard Knudsen cells. Unlike to the MBE growth of Bi_2Se_3 or Bi_2Te_3 films,^{14,16-17} we can obtain high quality stoichiometric Cr doped Sb_2Te_3 films with a (Sb, Cr)/Te flux ratio is only set about 1:3~1:2 and a substrate temperature set at 180°C . The typical growth rate in our experiment is ~ 0.33 QL/min, when the Sb and Te sources are set to 380°C and 260°C , respectively. **Fig.1a** shows the reflective high-energy electron diffraction (RHEED) patterns of the heat-treated

SrTiO₃(111) substrate for a $[2\bar{1}\bar{1}0]$ incident beam. The sharp reconstruction and clear Kikuchi lines demonstrate the high crystalline quality of the surface. **Fig. 1b** shows the RHEED patterns of 5 QLs Sb_{1.91}Cr_{0.09}Te₃ films on the SrTiO₃(111). A clear and sharp 1×1 pattern appears, and sharp streak-like RHEED patterns attest to a two dimensional (2D) layer-by-layer mode of thin film growth.¹⁴ In Cr doped Sb₂Te₃ films, the Cr atom neither substitutes on the anion site of Te nor enters inside the van der Waal gap, it only substitutes on the Sb site.^{8, 18}

To avoid possible ambient contamination of TI films, a 20nm-thick insulating amorphous Te capping layer was deposited on top at low temperature $T\sim 150\text{K}$ prior to taking the films out of the UHV chamber. Both the Te capping layers and the substrates are excellent electrical insulators, so their contributions to electrical transport can be safely neglected in electrical transport measurements. After removing the films from the chamber, 10nm Ti and 100nm Au electrodes were deposited through a shadow mask on the top of the sample to make ohmic contact, and to form Hall bar geometry. Low temperature silver conductive adhesive was overlaid on the bottom of the SrTiO₃(111) as a bottom gate electrode. The final millimeter-sized transistor devices are schematically shown in **Fig.1c**.¹⁹ Robust long-range ferromagnetic states in our Cr doped Sb₂Te₃ films were demonstrated through both electrical transport measurements (**Fig.1d**) and direct magnetization measurements with a superconductivity quantum interference device (SQUID) magnetometer (**Fig.1e**). **Fig.1d** shows T dependent Hall traces of 10QL Sb_{1.7}Cr_{0.3}Te₃ films. Clear square hysteresis loops at low temperatures ($T<55\text{K}$) show that the 10QL Sb_{1.7}Cr_{0.3}Te₃ films are in a ferromagnetic state. The inset of **Fig.1d** is a longitudinal resistance (R_{xx}) vs T curve, which shows a local maximum (hump) around 55K. Such behavior in the R_{xx} - T curve is due to spin disorder scattering that sets in at the paramagnetism-to-ferromagnetism transition. This scattering indicates the magnetic ordering temperature, known as the Curie temperature (T_C).⁹ T_C of 10QL Sb_{1.7}Cr_{0.3}Te₃ films is $\sim 55\text{K}$. **Fig.1e** shows the magnetization-field curves of 100QL Cr_{0.22}Sb_{1.78}Te₃ films. These curves show perfect hysteresis loops, where the magnetic moment per Cr

ion is determined by the saturation magnetization to be $\sim 3.4\mu_B$. This indicates that Cr atoms in the films form Cr^{3+} ions. The inset of **Fig.1e** shows the temperature dependent remanent magnetization exhibits an abrupt upturn around $T \sim 40\text{K}$. This indicates the T_C of 100QL $\text{Cr}_{0.22}\text{Sb}_{1.78}\text{Te}_3$ films is $\sim 40\text{K}$. T_C can be increased to high temperature with increasing Cr content in matrix of Sb_2Te_3 .

The evolution of electronic band structure resulting from different Cr concentrations in 5QL $\text{Sb}_{2-x}\text{Cr}_x\text{Te}_3$ films on SrTiO_3 (111) has been revealed by *in situ* angle-resolved photoemission spectroscopy (ARPES) measurements. All ARPES band maps were taken along the $\bar{\text{K}}-\bar{\Gamma}-\bar{\text{K}}$ direction at $T \sim 150\text{K}$. To avoid sample charging during ARPES measurements, a 300-nm-thick titanium (Ti) film is deposited at both ends of the substrate. Once a continuous film is formed, the sample is grounded to the sample holder through the contacts.¹⁴ **Fig.2a** shows the ARPES band spectrum of pure Sb_2Te_3 , which has well defined DSSs and a DP that lies at 65meV above the E_F .¹⁸ Different doping levels ($x \sim 0.05, 0.09$ and 0.14) were measured, and **Figs.2b** to **2d** show that the Cr doping causes insignificant changes to the DSSs. The topological DSSs persist with increasing x ; meanwhile, the energy difference between the DP and E_F becomes moderately larger with increasing x . This result demonstrates that a small number of hole-type carriers are introduced by Cr doping.

Electrical transport measurements have been performed in a cryostat with magnetic field ($\mu_0 H$) up to 15T and T down to 1.5 K, respectively. The Hall resistance (R_{yx}) and R_{xx} were measured using a standard ac lock-in method with the current parallel to the film plane and the magnetic field applied perpendicular to the film. A series of samples with progressively increasing content of Cr doping and electric field gating strengths were measured. Hall traces show that all $\text{Sb}_{2-x}\text{Cr}_x\text{Te}_3$ films have hole-type carriers and display a similar gate field-effect on anomalous Hall resistance. Because of these similarities, we take $x = 0.09$ as an example system, and all further data presented here is recorded from this sample.

Fig.3a shows $\mu_0 H$ dependence of the R_{yx} at $T = 1.5\text{K}$ in the series of gate voltages $V_g = -210\text{V}, -100\text{V}, -50\text{V}, 0\text{V}, +50\text{V}, +100\text{V},$ and $+210\text{V}$. Clear hysteresis loops show

that the 5QL $\text{Sb}_{1.91}\text{Cr}_{0.09}\text{Te}_3$ films are in a robust long-range ferromagnetic state. The hysteresis loops also indicate that the easy magnetization axis is perpendicular to the film, which is more useful for spintronic devices applications compared with an in-plane easy magnetization axis.⁸ The vertical intercept of the hysteresis loop becomes larger when V_g changes from -210V to +210V; the vertical intercept at $V_g=+210\text{V}$ is about twice of that at $V_g=-210\text{V}$. The inset of data in **Fig.3a** shows the R_{xx} vs V_g at $T=1.5\text{K}$, and shows that R_{xx} increases as V_g increases. Assuming a constant mobility, we can conclude that the total n_{2D} becomes lower with V_g from -210V to +210V. In a 2D system, the total R_{yx} can be defined as $R_{yx}=R_A \cdot M + R_O \cdot \mu_0 H$. Here R_A is the anomalous Hall coefficient, R_O is the ordinary Hall coefficient, M is the magnetization perpendicular to the film. In the low magnetic field limit, the anomalous Hall effect component dominates the Hall resistance; whereas in the high magnetic field limit the ordinary Hall effect component dominates the Hall resistance. The anomalous Hall resistance (R_{AH}) is determined by the extrapolation of the component linear in magnetic field. The slope of R_{yx} vs $\mu_0 H$ curve at low T under high magnetic field, where magnetization saturates, determines the type of conducting carriers and the total n_{2D} . In our samples, this deviation from the linear behavior occurs below 1T, which coincides with the saturation field of magnetization. R_{AH} and the total n_{2D} as a function of V_g at $T=1.5\text{K}$ are displayed in **Fig.3b**. Both R_{AH} and n_{2D} show a V_g dependence. R_{AH} changes from 24.1 Ω to 40.8 Ω , and n_{2D} changes from $3.4 \times 10^{14} \text{cm}^{-2}$ to $9.7 \times 10^{13} \text{cm}^{-2}$ as V_g increases from -210V to +210V. Intriguingly, R_{AH} increases as n_{2D} decreases. This phenomena, which results from a giant van Vleck magnetic susceptibility of valence electrons in TI systems,¹⁰ is different from the mechanism of ferromagnetism in conventional DMSs (*e.g.* (Ga,Mn)As) in which the carrier mediated and Ruderman-Kittel-Kasuya-Yosida (RKKY) interactions are responsible for the appearance of ferromagnetism and lead to a positive correlation between R_{AH} and n_{2D} .²⁰⁻²¹

Figs.4a to c display the variation of R_{yx} vs $\mu_0 H$ with gate voltages $V_g = -100\text{V}, 0\text{V}, +210\text{V}$, and T varied from 1.5K to 50K. Clear hysteresis loops can be observed in the region $1.5\text{K} \leq T < 15\text{K}$. As T increases the hysteresis loops vanish and the Hall traces

display nonlinear behavior at low field ($15\text{K} \leq T < 25\text{K}$). At $T \geq 25\text{K}$ the nonlinearity vanishes and the Hall traces become linear. The insets in **Figs. 4a to c** show the R_{xx} vs T curves for $V_g = -100\text{V}, 0\text{V}, +210\text{V}$. The film is metallic at $V_g = -100\text{V}$, but it displays insulating behavior at $V_g = +210\text{V}$. All three R - T curves show an increase in R at low temperature due to gap opening induced by ferromagnetism at low temperature.⁹

The T dependence of the remnant resistance (R_H) in R_{yx} at $\mu_0 H = 0\text{T}$ at $V_g = -100, 0, +210\text{V}$ is shown in **Fig.5a**. There is little change in T_C as V_g is varied at $T = 12.5\text{K}$ and $T = 15\text{K}$. The inset of **Fig.5a** displays a typical Arrot plot of the film, at $V_g = 0\text{V}$. The Arrot plot accurately confirms the occurrence of ferromagnetic state, since the effect of magnetic anisotropy and domain rotation can be minimized. The intercept of the high field isotherms of R_{yx}^2 vs H/R_{yx} give the spontaneous R_{yx} at $\mu_0 H = 0$. The isotherm at T_C passes through the origin (0, 0) point, and a negative intercept of an isotherm means no magnetization. The T_C s of the film at these three V_g s are all close to 15K, as the intercept of the linear component of the fits to the R_{yx}^2 vs H/R_{yx} curves around 15K is very close to the origin.²³ The temperature dependence of coercivity field strength (H_c) of the film at $V_g = -100, 0, +210\text{V}$ is shown in **Fig.5b**. The values of H_c , and therefore also the saturation magnetizations, are almost identical at constant T with variation in V_g . The saturation magnetizations at three V_g s are near 130mT along the easy magnetization axis. **Fig.5c** shows the 2D ordinary Hall coefficient, R_O^{2D} , as a function of T . R_O^{2D} can be expressed as $R_O^{2D} = \frac{1}{n_{2D}H}$. The T dependence of

n_{2D} is obtained from this expression, and we see that n_{2D} initially decreases, and then increases with the decreasing temperature below $T = 20\text{K}$. This T dependence is the typical behavior of conventional semiconductors.

To summarize, an insensitive DSS and a robust long-range ferromagnetic state have been unveiled in ultrathin epitaxial films of Cr doped Sb_2Te_3 . These characteristics were confirmed by *in situ* ARPES measurements and the presence of hysteresis loops in the anomalous Hall effect and SQUID magnetometer, respectively. We can tune the anomalous Hall effect through the effective bottom field-effect gate. While R_{yx} increases with the decreasing n_{2D} , H_c is not significantly changed. This

indicates a robust long-range ferromagnetic state that is insensitive to the carrier type and density, which is different from the ferromagnetic order mechanism in conventional DMSs. Because of this weak, carrier independent ferromagnetism in Cr doped Sb_2Te_3 , we chose Cr doped Sb_2Te_3 as the base candidate TI material to successfully realize the QAH effect.^{12, 18} This work also paves an effective path for controlling anomalous Hall voltage of magnetically doped TI thin films in future dissipationless TI-based magneto-electronic and spintronic devices.

Acknowledgment

We thank R. Wu for fruitful discussions. This work was supported by the National Natural Science Foundation of China, the ministry of Science and Technology of China, and the Chinese Academy of Sciences.

References

1. M. Z. Hasan and C. L. Kane, Rev. Mod. Phys. 82, 3045-3067 (2010).
2. X. -L. Qi and S. -C. Zhang, Rev. Mod. Phys. 83, 1057 (2011).
3. J. E Moore. Nature 464, 194-198 (2010).
4. H.J. Zhang, C. X. Liu, X. L. Qi et al. Nature Phys. 5, 438-442 (2009).
5. D. Hsieh et al. Phys. Rev. Lett. 103, 146401 (2009).
6. G. Wang et al. Nano Res. 12, 874-880(2010).
7. Y. P. Jiang et al. Phys. Rev. Lett. 108, 066809 (2012).
8. Y. J. Chien, thesis, University of Michigan, Ann Arbor, MI (2007).
9. Y.L. Chen et al. Science 329, 659-662 (2010).
10. R. Yu et al. Science 329, 61-64 (2010).
11. X. L. Qi et al. Phys. Rev. B 78, 195424 (2008).
12. C. Z. Chang et al. Science 340, 167 (2013).
13. X. L. Qi et al. Science 323, 1184(2009).
14. C. Z. Chang et al. SPIN 1, 21 (2011).
15. J. Chen et al. Phys. Rev. Lett. 105, 176602 (2010).
16. Y. Zhang et al. Nat. Phys. 6, 584 (2010).
17. Y. Y. Li et al. Adv. Mater. 22, 4002 (2010).

18. C. Z. Chang et al. *Adv. Mater.* 25, 1065 (2013).
19. M. H. Liu et al. *Phys. Rev. B* 83, 165440 (2011).
20. H. Ohno et al. *Nature* 408, 944-946(2000).
21. D. Chiba et al. *Appl. Phys. Lett.* 89, 162505(2006).
22. H. Ohno. *Science* 281, 951 (1998).
23. A. Arrott. *Phys. Rev.* 108, 1394 (1957).

Figures and figure captions

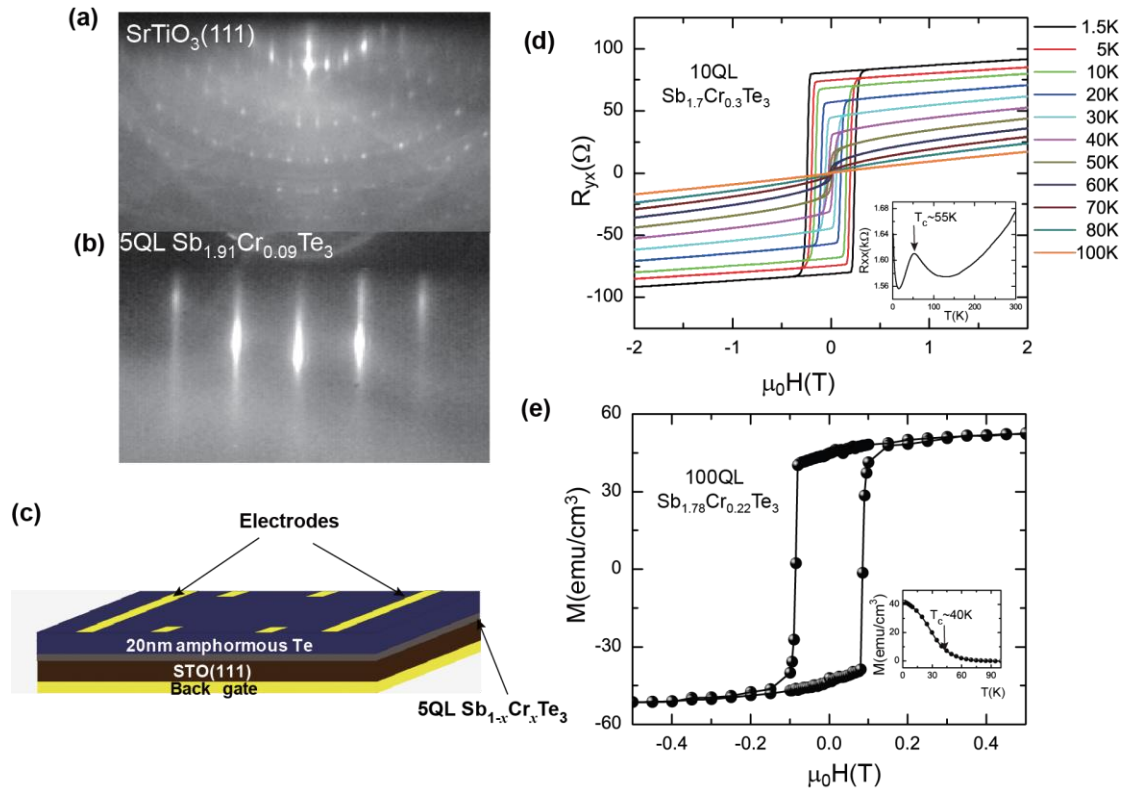


Fig.1 RHEED patterns of (a) heat-treated SrTiO₃(111) and (b) 5QL Sb_{1.91}Cr_{0.09}Te₃ films. (c) Schematic of the 5QL Cr-doped Sb₂Te₃ films for the transport measurements (the thickness is not to scale). (d) Magnetic field ($\mu_0 H$) dependent Hall resistance (R_{yx}) of the 10 QL Sb_{1.7}Cr_{0.3}Te₃ films at varied temperature, inset, the longitudinal resistance (R_{xx}) vs T curve. (e) SQUID hysteresis loops of 100QL Sb_{1.78}Cr_{0.22}Te₃ at $T=2$ K, inset, T dependent remanent magnetization (M) curve.

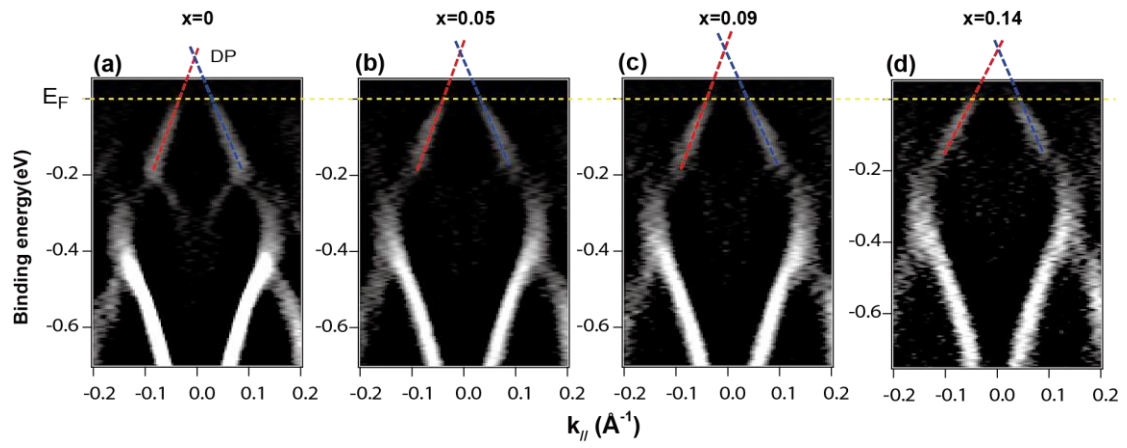


Fig. 2 ARPES band spectra of $\text{Sb}_{2-x}\text{Cr}_x\text{Te}_3$ taken along the $\bar{\text{K}}-\bar{\Gamma}-\bar{\text{K}}$ direction at $T \sim 150\text{K}$ for: **(a)** $x=0$; **(b)** $x=0.05$; **(c)** $x=0.09$; and **(d)** $x=0.14$.

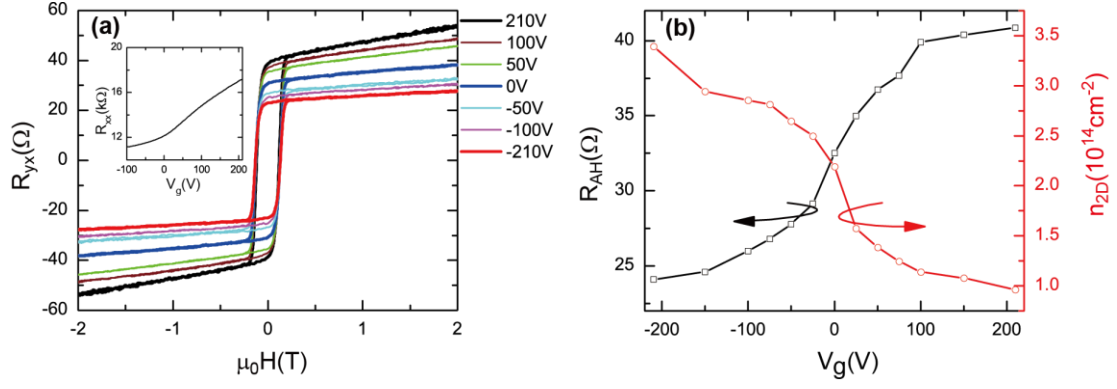


Fig.3 μ_0H dependence of the Hall traces of 5QL $\text{Sb}_{1.91}\text{Cr}_{0.09}\text{Te}_3$ at $T=1.5\text{K}$ with different gate bias (V_g). **(a)** R_{yx} vs μ_0H curves for V_g from -210V to $+210\text{V}$. Inset, R_{xx} vs V_g curve at $T=1.5\text{K}$. **(b)** The anomalous Hall resistance (R_{AH}) and the carrier density (n_{2D}) as a function of V_g .

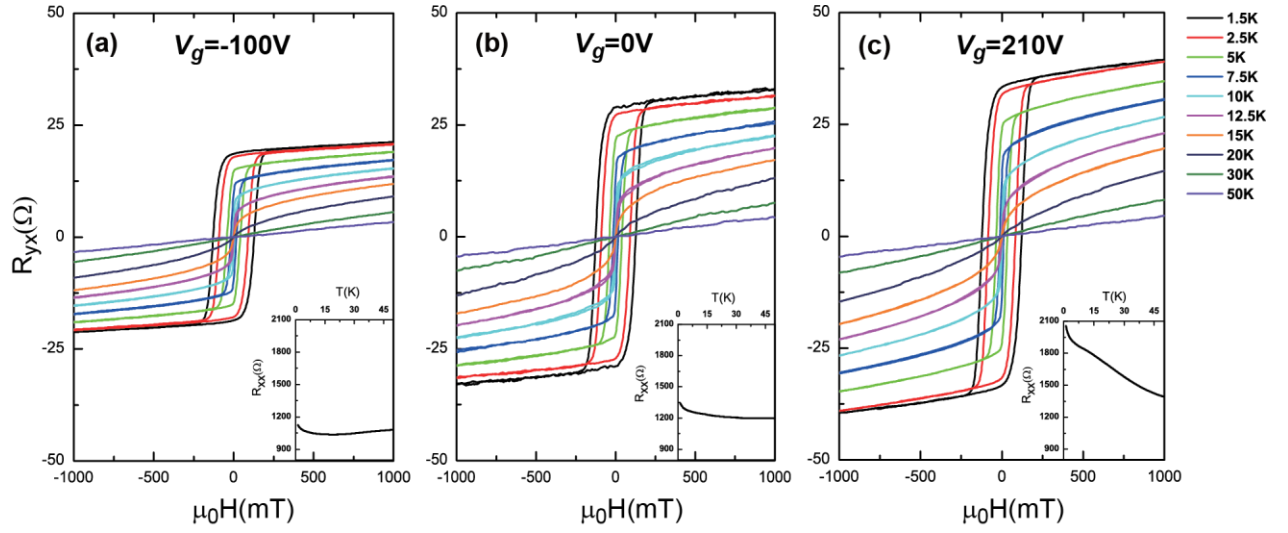


Fig.4 μ_0H dependence of the R_{yx} at varied T for (a) $V_g = -100V$, (b) $0V$ and (c) $+210V$. Insets of (a), (b) and (c), are the respective the R_{xx} vs T curves.

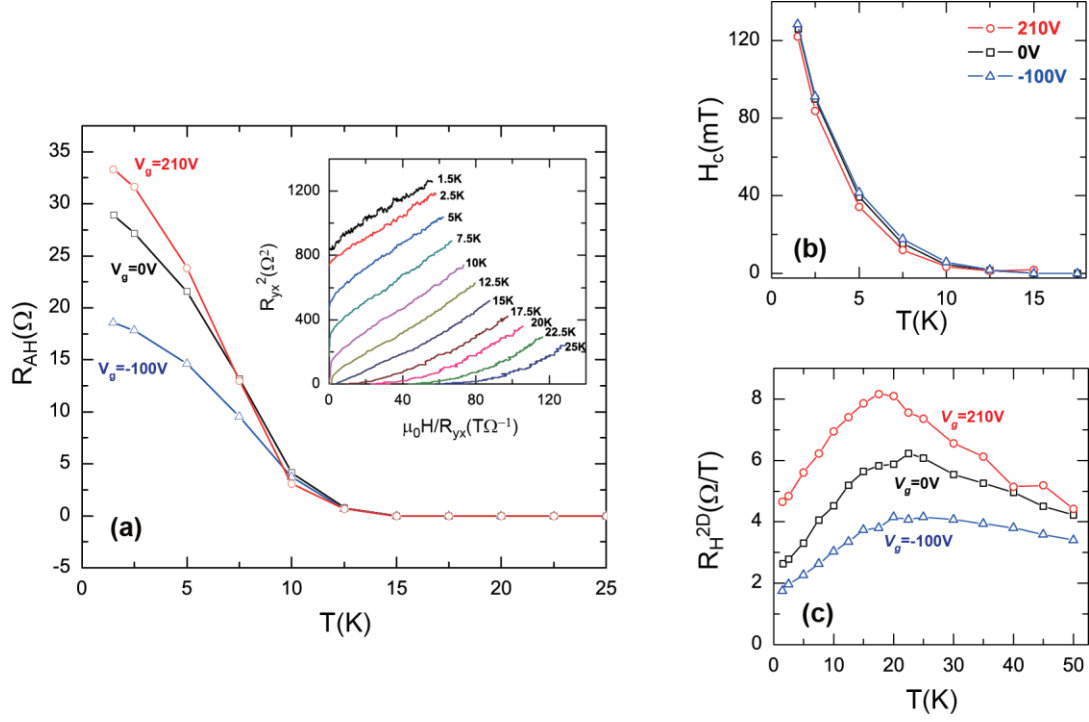


Fig.5 (a) T dependence of spontaneous Hall resistance (R_H) for $V_g = -100V$, $0V$ and $+210V$. Inset, Arrot plots for the samples at $V_g = 0V$. (b) T dependence of coercivity field (H_c) for $V_g = -100V$, $0V$ and $+210V$. (c) T dependence of the ordinary Hall coefficient (R_H^{2D}) for $V_g = -100V$, $0V$ and $+210V$. Data at $V_g = -100V$, $0V$ and $+210V$ are shown by blue up triangles, black squares and red circles, respectively.